




Article

Examining Wear Mechanisms in Railway Wheel Steels: Experimental Insights and Predictive Mapping

Nicola Zani , Angelo Mazzù , Luigi Solazzi *  and Candida Petrogalli

Department of Mechanical and Industrial Engineering, University of Brescia, Via Branze, 38, 25123 Brescia, Italy; nicola.zani@unibs.it (N.Z.); angelo.mazzu@unibs.it (A.M.); candida.petrogalli@unibs.it (C.P.)

* Correspondence: luigi.solazzi@unibs.it; Tel.: +39-030-3715577

Abstract: Railway systems play a pivotal role in modern transportation networks, contributing to both efficiency and environmental sustainability. This study investigated the multifaceted aspects of wear phenomena in railway engineering, focusing on their significant implications for environmental costs and operational efficiency. Experimental trials were conducted using a high-performance bi-disc apparatus, evaluating a range of materials, contact pressures, and lubrication conditions. Shakedown maps were employed to assess ratcheting behaviour, while the wear rate was analysed as a function of the fatigue index (*FI*). The results reveal the intricate interplay of contact pressure, slip ratio, material properties, and lubrication in determining wear and ratcheting behaviour. Oxidative and mild wear mechanisms were identified, and wear debris composition and morphology were characterised. The outcomes from this research clarify the pivotal role that wear processes play within railway systems and the far-reaching environmental repercussions they entail. This exploration contributes to the ongoing optimisation of railway operations, offering valuable insights aimed at mitigating unavoidable pollution sources and strengthening sustainability efforts. By delving into the intricate dynamics of wear phenomena within wheel–rail material, this research paves the way for innovative solutions that not only enhance operational efficiency but also minimise the ecological footprint of railway transportation.

Keywords: wear mapping; rolling contact; fatigue index; railway wheel



Citation: Zani, N.; Mazzù, A.; Solazzi, L.; Petrogalli, C. Examining Wear Mechanisms in Railway Wheel Steels: Experimental Insights and Predictive Mapping. *Lubricants* **2024**, *12*, 93. <https://doi.org/10.3390/lubricants12030093>

Received: 12 February 2024

Revised: 23 February 2024

Accepted: 2 March 2024

Published: 14 March 2024



Copyright: © 2024 by the authors. Licensee MDPI, Basel, Switzerland. This article is an open access article distributed under the terms and conditions of the Creative Commons Attribution (CC BY) license (<https://creativecommons.org/licenses/by/4.0/>).

1. Introduction

Railway engineering remains steadfast in its commitment to modernising operations, with a primary focus on improving efficiency and championing environmental advantages. In line with this mission, a 2019 estimate provided by the European Union revealed staggering collective costs linked to air pollution, climate change, and noise pollution stemming from railway transportation, reaching an approximate sum of 7.8 billion euros [1]. Beyond mere statistics, trains are implicated in the degradation of soil and water quality through a multitude of mechanisms, including brake, wheel, and rail abrasion, fuel combustion, and numerous other sources of pollution. Such multifaceted impacts underscore the pressing need for continued innovation and sustainable practices within the railway industry as it navigates the complexities of modern transportation while striving for a cleaner, more eco-friendly future. Some of these effects may be mitigated; for example, a diesel-powered train can be replaced by one powered by renewable resources. However, other sources of pollution such as wear cannot be avoided. Therefore, understanding the wear processes accountable for releasing metals into the environment is crucial in reducing this unavoidable pollution source.

Over time, there has been extensive research conducted on wheel–rail wear. Several researchers have conducted laboratory tests (small-scale) [2–11] and field experiments [12–19]. The former are usually preferred because of their cost-effectiveness and more accurate investigation of the material responses at the expense of the dynamic responses (lateral

forces). Furthermore, small-scale tests allow for replicating both clean and contaminated contact (wet contact [20–25] or in the presence of solid contaminants [26–34]) and for better controlling creepage.

Wear is affected by several phenomena, such as shear stress at the contact [35,36], wheel material (hardness and microstructure) [10,37–46], lubricants and debris [47–49], temperature [50–54], polygonization [55–59], and surface treatments [60–64]. In actual wheels, polygonization is caused by wheel–rail coupled vibration, and material loss is a result of the wheel–rail coupled vibration. Once the wheel tread is polygonised, a reprofiling operation should be planned, reducing the wheel life [3,65]. In small-scale tests (like bi-disc), as well as in wheels, potential stochastic out of roundness may be ascribed to anomalous wear damage distribution on the surface due to the presence of intermediate-bainitic structures in ferritic–pearlitic microstructure [66]. Conversely, wear has a beneficial effect on the service life by eliminating surface cracks resulting from rolling contact fatigue [3,65,67–69].

Numerous research efforts have focused on mapping and modelling wear behaviour.

For example, Bolton and Clayton [70] proposed an approach based on the dissipated energy responsible for wear, defined as $T\gamma/A$, where T , γ , and A are the traction force, creepage, and contact area, respectively. This parameter was plotted against the wear rate, calculated as the mass loss in μg divided by rolling distance in meters and the contact area in mm^2 . This approach identified three wear regimes: mild, severe, and catastrophic [70–76]. The wheel tread and railhead are subjected to mild wear, while the wheel flange and rail gauge corner typically fall within the severe and catastrophic regimes. In the mild wear regime (low $T\gamma/A$), oxidative wear occurs, and abrasive score marks are visible because of the braking of the oxidative layer. At high $T\gamma/A$, the wear mechanisms are activated by a ratcheting process followed by a shear fracture that generates metallic flake-like particles. Oxidative wear is characterised by a predominant quantity of iron oxides among the debris; as one transitions from the oxidative regime to the mild regime and finally to the severe and catastrophic regimes, the percentage of oxide decreases in favour of iron particles [70,77–79]. Figure 1 [70] explains the wear mechanisms according to the $T\gamma/A$ approach.

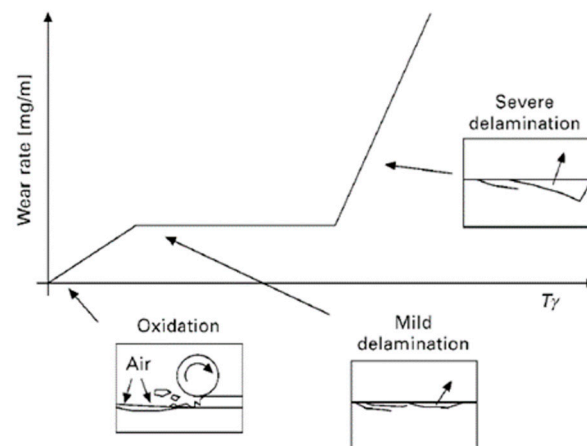


Figure 1. Wear mechanisms according to the $T\gamma/A$ approach.

Lim and Ashby [80] and Lewis and Olofsson [71] also proposed mapping sliding wear mechanisms using Archard's equation [81]:

$$K_W = \frac{VH}{FL} \quad (1)$$

where K_W is the wear coefficient, V is the wear volume, F is the normal load, H is the material hardness, and L is the sliding distance. The variable K_W is then plotted against the sliding speed and contact pressure, resulting in a 3D graph indicating the wear transition.

Rolling contact fatigue (RCF), in addition to wear damage, poses a threat to both the wheel and rail integrity. RCF occurs due to cyclic loading of the material, leading to the formation of cracks that have the potential to propagate and eventually result in component fractures. These fatigue cracks can originate either on the surface or in the sub-surface. Surface cracks emerge when the level of plastic deformation surpasses the critical strain, potentially leading to propagation facilitated by hydro-pressurisation and contact loading [3,65,82–84]. Although relatively rare, sub-surface cracks present significant risks, as they are invisible to the naked eye at their onset; defects such as oxides or sulphides in the sub-surface can facilitate crack initiation [65,85–89]. Despite being traditionally studied as separate phenomena, RCF and wear are closely interconnected. Reduced wear may facilitate the progression of cracks to the point of RCF failure, while if rolling contact fatigue cracks are interrupted, wear is more likely to prevail.

In the literature, shakedown maps were introduced to predict the fatigue response to cyclic loading [90–93]. An example of a shakedown map is illustrated in Figure 2 [90]. These maps plot the friction coefficient against the contact pressure normalised by the shear yield strength of the material. The four responses are elastic, elastic shakedown, plastic shakedown, and ratcheting. From a mathematical point of view, the fatigue index (FI) defines whether the material experiences ratcheting ($FI > 0$), calculated as follows:

$$FI = \mu - \frac{k}{P} \quad (2)$$

where μ is the friction coefficient, k is the cyclic shear yield strength, and P is the applied contact pressure.

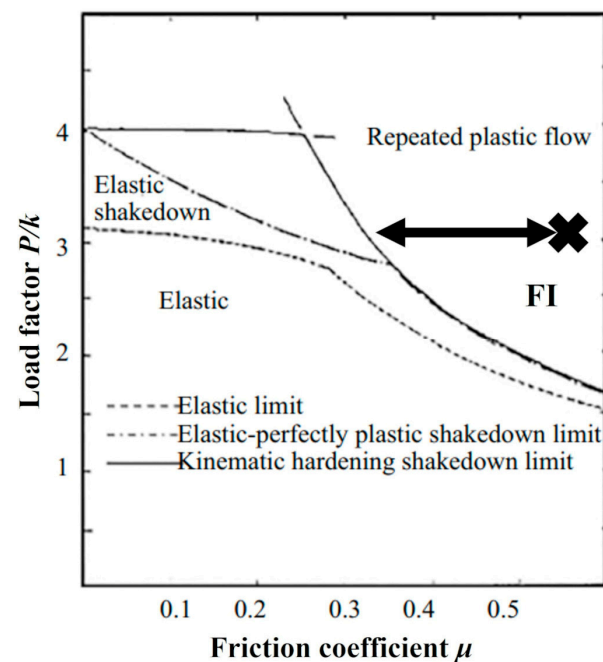


Figure 2. Example of a shakedown map for cylindrical contact.

Vicente et al. [94] were the first to utilise the fatigue index (FI) to establish a correlation between wear damage and rolling contact fatigue in twin-disc tests conducted under various conditions, including different specimen thicknesses, normal pressures, and creepage. Their study revealed an exponential relationship between wear rate and the fatigue index. Zani and Petrogalli [95] explored the correlation between FI , wear rate, and shear yield strength. They conducted bi-disc rolling contact tests at a nominal Hertzian contact pressure equal to 1100 MPa, varying parameters such as steel type (European and American) and disc extraction location; furthermore, they investigated three kinds of contact conditions:

clean, with sand particles, and lubricated with water mixed with glycol. They found that sand contaminants and water lubrication led to a reduction in *FI*, although the wear rate significantly increased when solid particles were present between the discs. In clean contact conditions, the wear rate decreased with increasing hardness and yield strength. Similarly, Zani and Petrogalli [95] focused on the wear mechanisms according to the contaminants (adhesive or abrasive wear); however, no details about the wear regimes were provided.

This study delved deeper into the relationship between wear and rolling contact fatigue (RCF) in the contact between railway rails and wheels. It paid special attention to how different types of wear are influenced by factors like slip ratio, lubrication, and contact pressure. Additionally, the research analysed the characteristics of the wear debris, including its type, distribution, and composition. By focusing on these aspects, the study aimed to provide a comprehensive understanding of how wear interacts with RCF in railway systems, ultimately contributing valuable insights to enhance railway maintenance and performance.

2. Experimental Details

This research showcased findings derived from experimental tests conducted utilising the advanced bi-disc apparatus situated at the University of Brescia. Figure 3 illustrates the setup of the apparatus. The system was outfitted with two mandrels, one of which was positioned on linear air slides, operated independently by two alternating current (AC) 33 kW motors capable of reaching speeds of 1200 rpm. A servo-hydraulic actuator was utilised to generate the contact load and manage the approach motion, with a capacity of 75 kN. Speed, torque, and normal load were recorded at a sampling frequency of 5 Hz using a dedicated National Instruments data acquisition system.

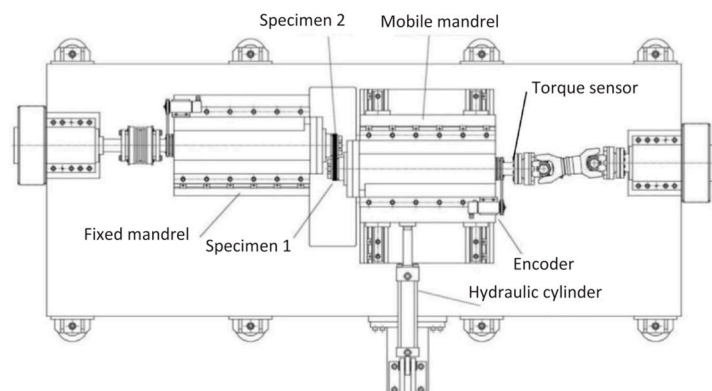


Figure 3. Twin-disc testing machine.

The cylindrical test specimens were machined from the wheel-tread and the railhead surfaces. The cylindrical test samples were extracted as close as possible to the contact surfaces to ensure mechanical properties were as independent as possible from mechanical property gradients induced by heat treatments. These wheel and rail discs had a diameter of 60 mm with a thickness of 15 mm. Since the specimens were cylindrical, the contact track width corresponded to the specimen thickness.

The wheel and rail disc specimens, made of pearlitic steels, were produced by the Italian company Lucchini RS. The considered wheel steels were AAR CLASS B, AAR CLASS C, SANDLOS[®] H, EN RT7, EN ER8, and SUPERLOS[®]. The first four steels comply with American Standards AAR M107/M208 [96], and the SANDLOS[®] steels are a specific group engineered explicitly for use in sandy environments [97]. The others refer to the European Standards EN 13262 [98], and SUPERLOS[®] is an upgrade of the traditional EN ER8 and EN ER9 steels [99]. The rail discs abide by Standard EN 13674-1 [100]. Table 1 delineates the mechanical properties of the investigated materials, accompanied by the bibliographic references from which the test outcomes have been sourced.

Table 1. Wheel and rail steels mechanical properties.

Component	Specimen	Ref.	Monotonic Yield Stress [MPa]	Cyclic Yield Stress [MPa]	HB
Wheel	R7T	[3]	420	350	247
	ER8	[22,23,26]	590–600	470	283
	SUPERLOS®	[22,23]	640	523	275
	AAR CLASS B	[23]	660	580	313
	AAR CLASS C	[26]	750	640	355
	SANDLOS®H	[26]	800	720	354
Rail	350 HT 900A	[26] [3,22,23]	470	390	300–350

The applied contact pressures were 700, 900, 1100, and 1300 MPa. All the tests were carried out at a constant creep ranging from 0% (pure rolling) to 3%. The rotational speeds were set so that the average disc speed was 500 rpm. The experiments were carried out in clean (C) and contaminated conditions (W), spraying water jet with 10% glycol to prevent corrosion. Table 2 summarises the applied operating conditions.

Table 2. Testing conditions.

Wheel Specimen	Pressure [MPa]	Slip Ratio [%]
R7T	700	0.06 (C), 0 (W)
	900	0 (C, W), 0.03 (C), 0.06 (C, W)
	1100	0 (C, W), 0.03 (C), 0.06 (W)
	1300	0.01 (C)
ER8	900	0 (C), 1 (C), 3 (C)
	1100	0 (C), 0.24 (W), 1 (C, W), 3 (C)
	1300	0 (C), 1 (C), 3 (C)
SUPERLOS®	1100	0.24 (W), 1 (C, W)
CLASS B	900	0 (C), 1 (C), 3 (C)
	1100	0 (C), 0.24 (W), 1 (C, W)
	1300	0 (C), 1 (C)
CLASS C	900	0.5 (C), 1 (C), 3 (C)
SANDLOS® H	900	1 (C), 3 (C)
	1100	1 (C), 3 (C)
	1300	0 (C), 1 (C), 3 (C)

The specimens were ultrasonically cleaned and weighed at the beginning of the test using a precision balance with 0.001 g of resolution. The wear rate was first calculated as the difference between the initial specimen mass and the mass at the end of the test divided by the running distance and the contact area ($\text{g}/\text{m}/\text{mm}^2$), according to Archard's law. After the test, the contact surfaces were acquired using a DMS300 stereomicroscope equipped with a Leica digital camera (Wetzlar, Germany) and LAS 4.13 analyser software. Wear debris was analysed using a TNX powder diffractometer (Riva del Garda, Italy) following the UNI EN 13925-2-2006 [101] standard to identify the chemical composition, using a JEOL-6010 PLUS/LA (Tokyo, Japan) scanning electron microscope (SEM) to classify size and distribution.

3. Results and Discussion

Figure 4 portrays the shakedown maps for cylindrical contact and the experimental conditions (coefficient of friction and load factor $\frac{k}{p}$) in clean contact (Figure 4a,b) for European and American steels, respectively, and in lubricated contact (Figure 4c). The numerical values represented correspond to the percentages of the slip ratio. Fixing the

contact pressure and increasing the slip ratio generally causes the friction coefficient to rise, moving the operation point to a ratcheting area both in clean and lubricated contact. In clean contact, the American steels generally exhibit lower load factors than the European steels when tested under the same contact pressure. This is ascribed to the higher shear yield strength of American steels, translating into an increased likelihood of less-resistant steels being subjected to ratcheting (since the ratcheting area widens with the strength reduction). As the shakedown is increasingly overcome, more plastic deformation accumulates until failure occurs.

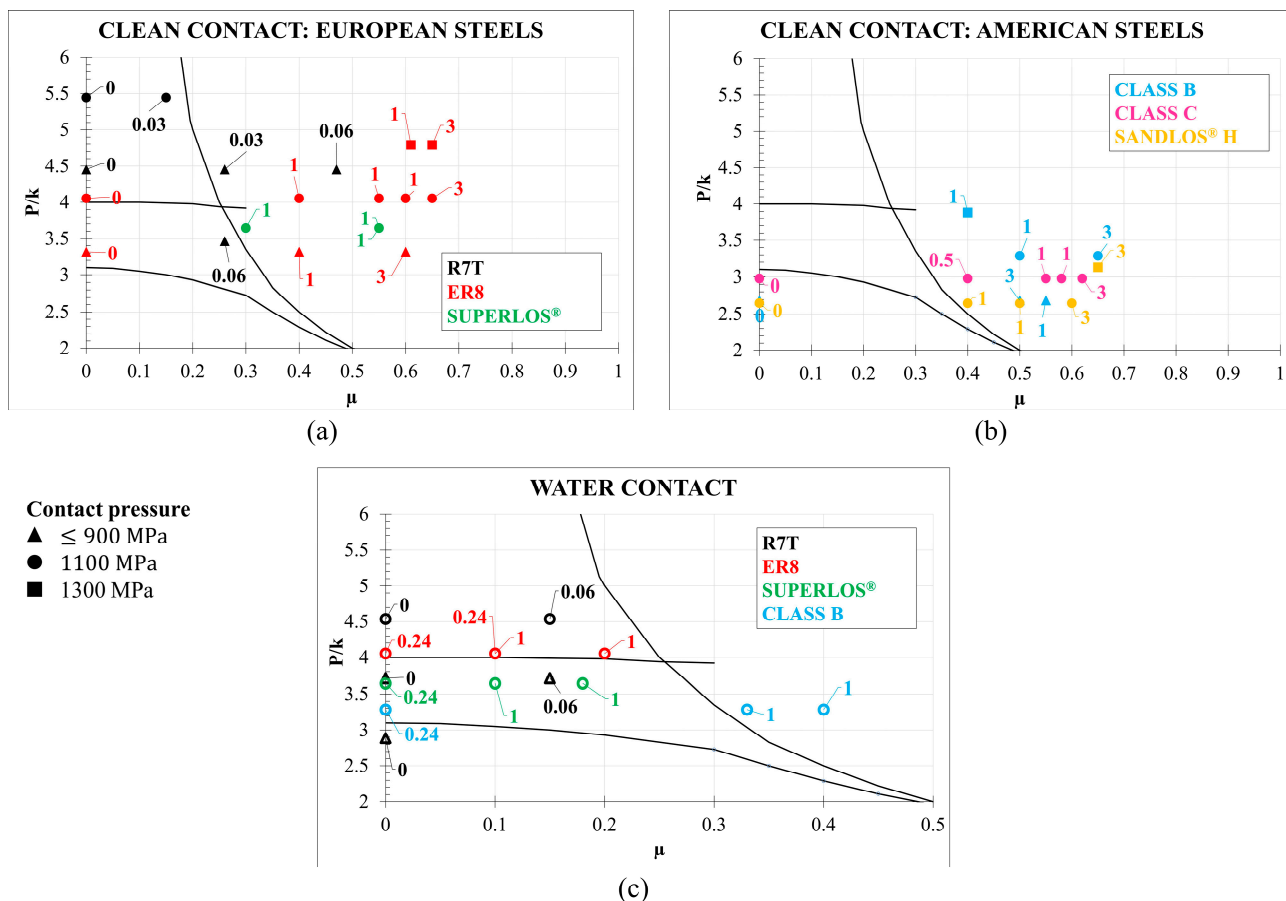


Figure 4. Shakedown map for cylindrical contact showing the operating conditions: (a) European wheels in clean condition, (b) American wheels in clean condition, and (c) European and American wheels in water condition.

Additional information given by the shakedown maps is the position of the maximum shear stress. When the coefficient of friction increases beyond a threshold of about 0.3, the maximum stress arises at the surface contact. In clean contact (R7T excluded), we conclude that, with a slip ratio higher than 1%, the surface layers of the samples undergo maximum stress and ratcheting. In contrast, for the water condition, the coefficient of friction was generally lower than 0.3; therefore, the maximum stress is in the sub-surface. In these circumstances, steel cleaned from defects, including those not visible to the naked eye, is essential. However, the lubricated tests were run with constant application of water. A different response would result if the same tests were conducted with the previous clean contact cycles to initiate cracking [102,103].

Figure 5 shows a map defined to predict the wear rate once the FI is known. Wherever the values of the wear rate were not available in the cited works, they were calculated according to Equation (1). We can distinguish clean contact from lubricated contact if we exclude the pure rolling condition. First, we notice that FI values in wet contact are

generally lower than in clean conditions, except for the pure rolling tests, which show similar *FI*s regardless of the lubrication. The lower *FI* in the lubricated tests can be ascribed to the lower friction coefficient. The wear rate increases with the slip ratio. In detail, in clean conditions, the wear rate increased by about four orders of magnitude, passing from the pure rolling to a slip ratio equal to 3%, while in the lubricated test, the wear rate increased by two orders of magnitude from a slip ratio of 0% to 1% [103].

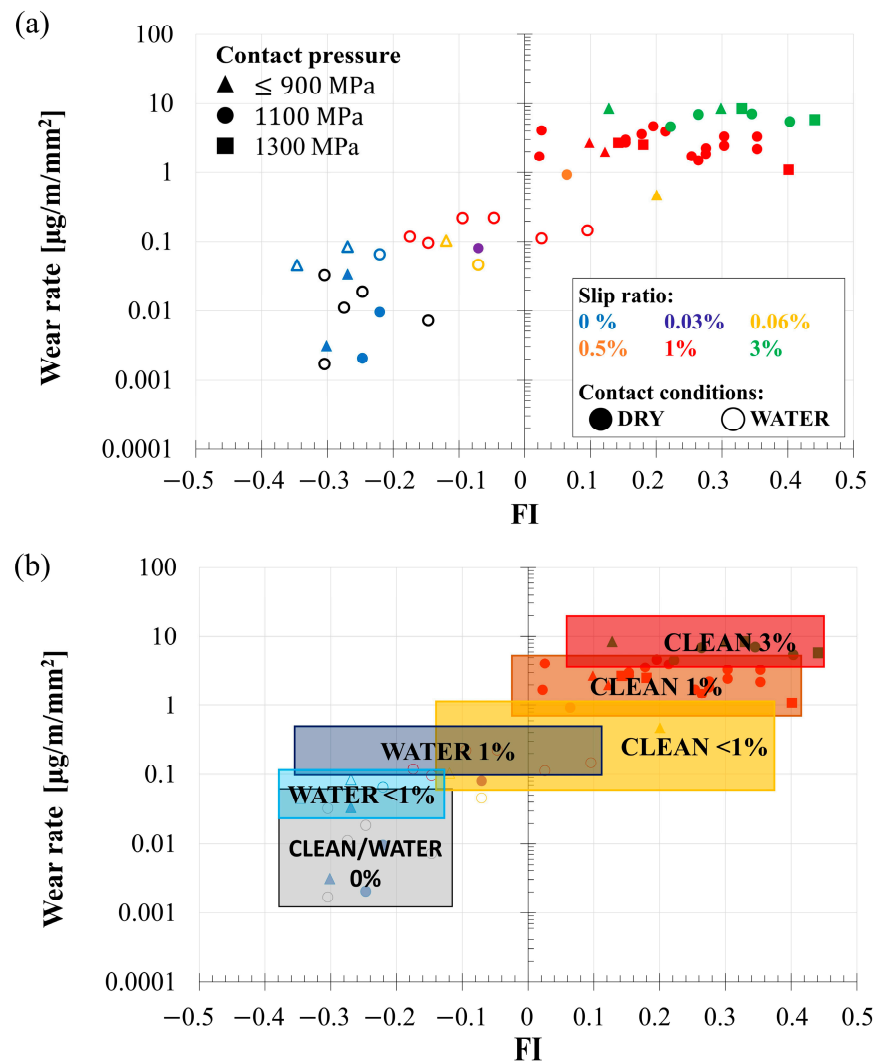


Figure 5. Wear rate evolution according to *FI* (a) for clean and lubricated tests showing the slip ratio and (b) a cluster map of the operating conditions.

The scattering in the *FI* values at a constant slip ratio does not seem to depend on the contact pressure, but it can be attributed to loose machine tolerances for the discs and differences in specimen roughness values and material properties.

Figure 6 shows similar results, focusing on the type of wheel steel. The wear trend in clean contact exhibits no clear differences. All the rail–wheel specimens were produced in the 2010s, apart from R7T, which dates to the previous decade. This difference is noticeable since the R7T steel tested at 900 MPa and a slip ratio of 0.06% yielded a *FI* comparable to that of the ER8 specimens tested at 1300 MPa and a slip ratio $\geq 1\%$. Moreover, had R7T been tested at 1300 MPa and slip ratios higher than 1%, its wear rate might have been higher than ER8. Figure 5 also shows that wear rates gradually decreased as new and improved materials were introduced. Indeed, the equivalent R7T produced by the same

company in the following years had higher mechanical properties, which would have led to lower *FIs*.

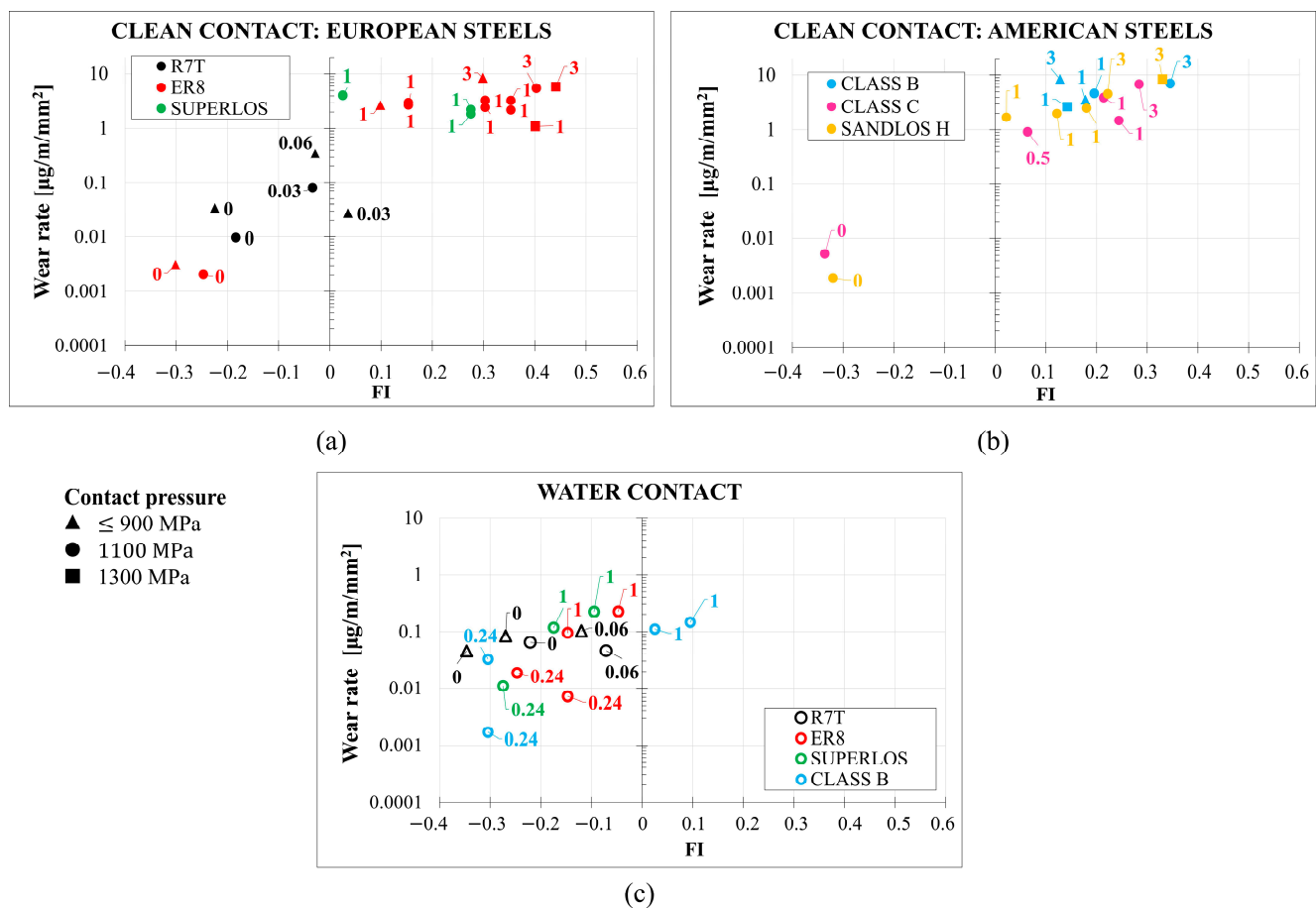


Figure 6. Wear rate evolution according to *FI* for (a,b) clean and (c) lubricated tests, according to the wheel material.

If we compare American and European steels tested in clean conditions, excluding a few cases, the American steels show lower *FIs* and slightly lower wear rates, likely because their hardness values are comparable to those of rail materials.

The *FIs* were generally less than zero in the lubricated tests, even with a 1% slip ratio and 1100 MPa of contact pressure. The only exception was CLASS B. Once again, R7T tested at lower contact pressures and slip ratios overlapped with the more recent steels tested at more critical conditions.

The wear rate was also examined based on the $T\gamma/A$ parameter (Figure 7). We found that the tested samples experienced either oxidative or mild wear, typically identified as a Mode I regime [70,72]. Samples tested in clean conditions and with pure rolling or slip ratios lower than 1% suffered from oxidative wear regardless of the contact pressure. Increasing the slip ratio led to the transition from oxidative to mild wear. When oxidative wear occurred, the wear rate was lower than $1 \mu\text{g}/\text{m}/\text{mm}^2$, while it varied between 1 and $10 \mu\text{g}/\text{m}/\text{mm}^2$ in the case of the mild regime.

The X-ray diffraction (XRD) spectra in Figure 8 illustrate that the main compositions of the wear debris tested in clean conditions at 1% are oxide (Fe_2O_3 , hematite) and iron at 36% and 64%, respectively; on the other hand, the debris tested at 3% mainly consists of iron. The presence of oxide in the analysed samples at 1% indicates that oxidative and mild wear mechanisms were triggered. Wear debris samples are shown in the SEM micrographs in Figure 9. The debris at 1% shows large, smooth, thin metallic flakes produced by mild-oxidative wear. The flakes were usually up to $100 \mu\text{m}$ in size; the debris of the samples

tested at 3% retained the flake morphology but was less regular and showed a greater range of particle sizes.

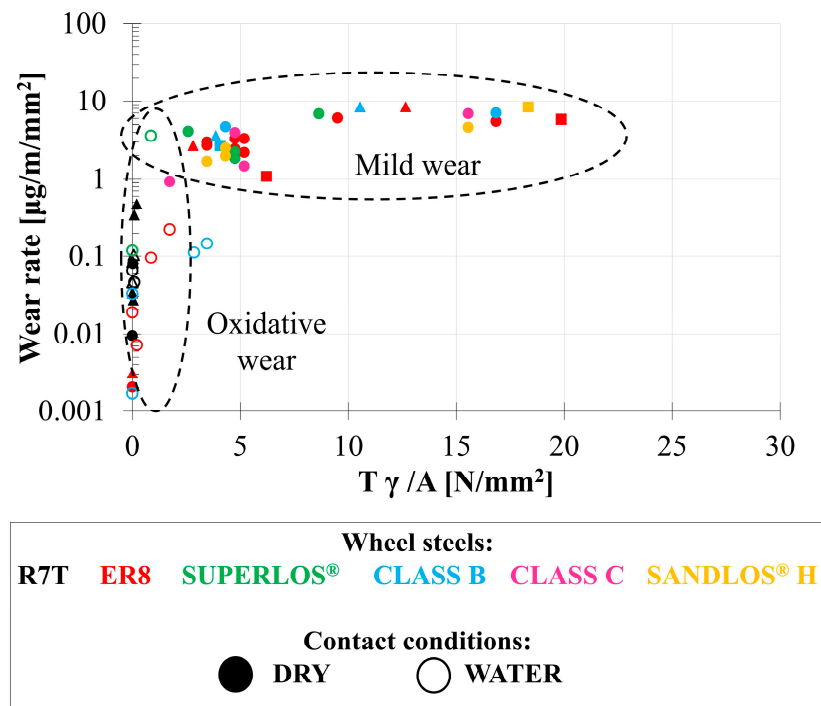


Figure 7. Wear regimes identified during bi-disc testing.

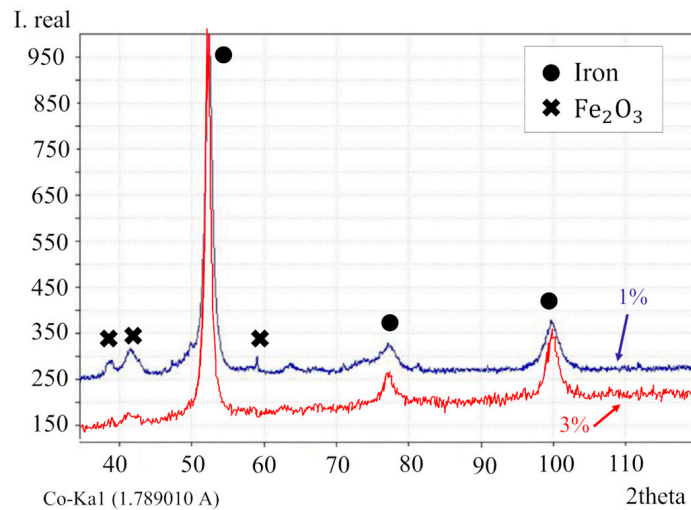


Figure 8. X-ray diffraction (XRD) spectra of wear debris collected from wheel and rail specimens under clean conditions.

To study the impact of the applied contact pressure and the slip ratio, Figure 10 shows the wear surface morphology under the dry condition for ER8, CLASS B, and SANDLOS®H wheel rollers. For the ER8 steel tested at 1%, the worn surface is characterised by ripples and metallic flakes whose dimensions reduced when the contact pressure increased; in contrast, the number of flakes increased with the contact pressure. SANDLOS®H and CLASS B experienced similar mechanisms.

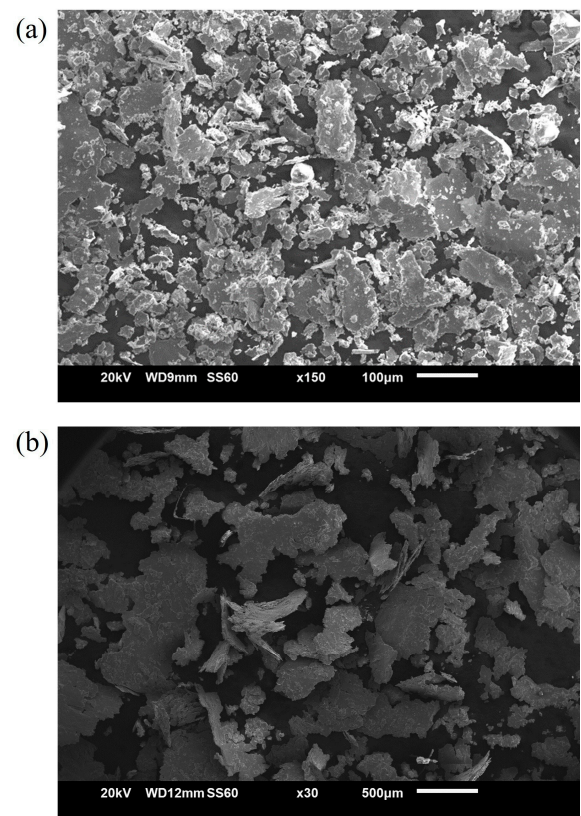


Figure 9. SEM micrographs of wear debris on the wheel–rail specimens in clean conditions: (a) samples tested at 1%, (b) samples tested at 3%.

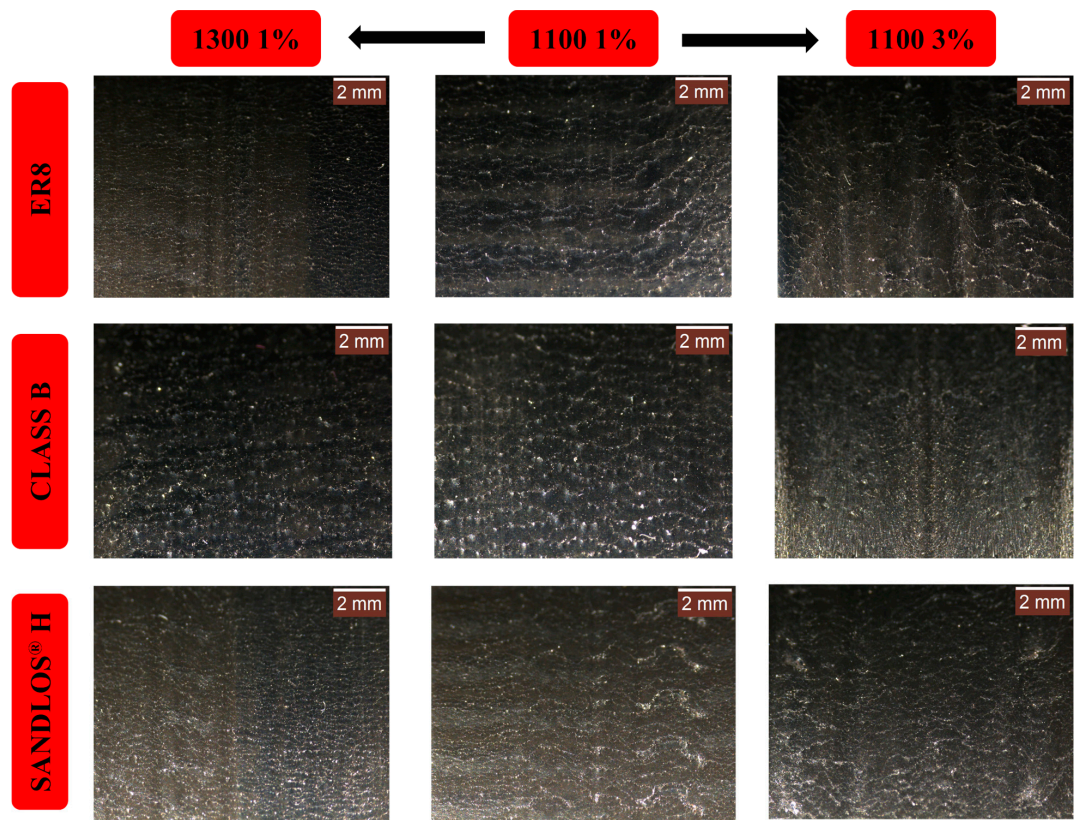


Figure 10. Wear surface produced by contact stresses of 1100 MPa (1% and 3%) and 1300 MPa (1%) in clean conditions for ER8, CLASS B, and SANDLOS®H (rolling direction from bottom to top).

However, in CLASS B, this mechanism was less pronounced; indeed, its wear behaviour was less affected by the load, as shown in Figure 4. On the other hand, when the slip ratio increased to 3%, the flake dimensions did not vary regardless of the type of steel, but the surface was smoother, as also witnessed by Bolton et al. [43].

As regards the lubricated contact, Figure 11 shows the tracks of ER8 and CLASS B tested at 1100 MPa and 1%. ER8 exhibited the detachment of material fragments, while CLASS B showed plastic deformation of the material in the direction of the load. This result confirms the position of these material points on the map in Figure 4c, showing that CLASS B underwent ratcheting while ER8 remained in shakedown.

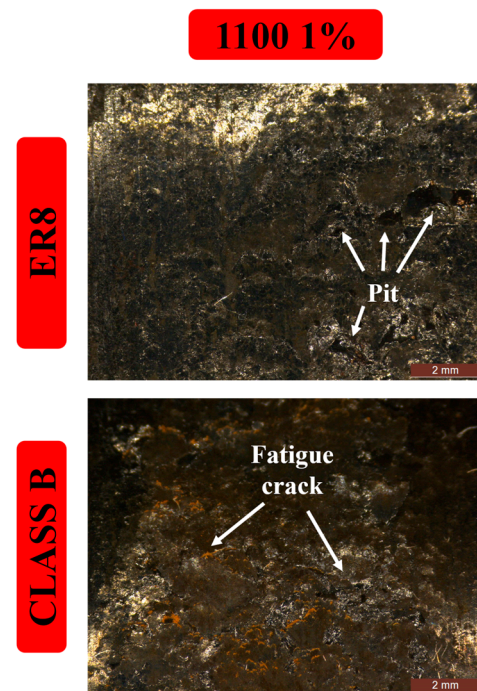


Figure 11. Wear surface produced by a contact stress of 1100 (1%) in wet conditions for ER8 and CLASS B (rolling direction from bottom to top).

4. Conclusions

This comprehensive study extensively explored and analysed the wear behaviour of various railway wheel pearlitic steels, examining their responses under a diverse array of contact pressures and lubrication conditions. Through this investigation, the research shed light on the intricate interplay between slip ratio, material properties, and wear rates, providing valuable insights for further understanding and optimisation. The following conclusions can be inferred:

- Clean contact conditions resulted in higher coefficients of friction and maximum stress at the surface, while lubricated contact conditions showed lower coefficients of friction and maximum stress in the subsurface.
- Wear rates increased with increasing slip ratio, with a significant increase observed in clean contact conditions compared to lubricated conditions.
- Introducing new and improved materials led to lower wear rates, indicating the importance of material selection in minimising wear in wheel–rail systems.
- Wear mechanisms were identified as oxidative and mild wear, with the presence of oxide and iron in wear debris in the former case and only the presence of iron in the latter, highlighting the role of lubrication and surface cleanliness in wear prevention.

These conclusions offer insights into the optimisation of wheel–rail system performance. Beyond their immediate applications, they hold profound significance for the advancement of predictive capabilities and the refinement of analytical models. By in-

forming material selection and lubrication strategies to minimise wear rates and enhance durability, these findings not only impact current railway engineering practices but also lay the groundwork for more accurate predictive models. The implications extend far beyond the laboratory, as they directly influence the calibration and validation of analytical models across diverse real-world applications. As such, this research plays a pivotal role in advancing the state of the art in predictive maintenance and reliability engineering, driving innovation and efficiency in railway systems.

Author Contributions: Conceptualisation, N.Z. and C.P.; methodology, N.Z., C.P., L.S. and A.M.; data curation, N.Z.; writing—original draft preparation, N.Z., C.P., L.S. and A.M.; writing—review and editing, N.Z., C.P., L.S. and A.M.; visualisation, N.Z., C.P., L.S. and A.M.; supervision, N.Z. All authors have read and agreed to the published version of the manuscript.

Funding: This work is supported by the European Union-FSE-REACT-EU, PON Research and Innovation 2014–2020 DM1062/2021 contract number n. 46-G-13219-1 (Prot. N. 0002702., 12/2022).

Data Availability Statement: Data are available upon request from the authors.

Conflicts of Interest: The authors declare no conflict of interest.

References

1. European Environment Agency. *Transport and Environment Report 2020: Train or Plane?* European Environment Agency: Copenhagen, Denmark, 2020; Volume 19.
2. Šmach, J. Two Contributions to Rolling Contact Fatigue Testing Considering Different Diameters of Rail and Wheel Discs. *Lubricants* **2023**, *11*, 504. [\[CrossRef\]](#)
3. Donzella, G.; Mazzù, A.; Petrogalli, C. Competition between wear and rolling contact fatigue at the wheel-rail interface: Some experimental evidence on rail steel. *Proc. Inst. Mech. Eng. Part F J. Rail Rapid Transit* **2009**, *223*, 31–44. [\[CrossRef\]](#)
4. Hardwick, C.; Lewis, R.; Eadie, D.T. Wheel and rail wear—Understanding the effects of water and grease. *Wear* **2014**, *314*, 198–204. [\[CrossRef\]](#)
5. Leso, T.P.; Siyasiya, C.W.; Mostert, R.J.; Moema, J. Study of rolling contact fatigue, rolling and sliding wear of class B wheel steels against R350HT and R260 rail steels under dry contact conditions using the twin disc setup. *Tribol. Int.* **2022**, *174*, 107711. [\[CrossRef\]](#)
6. Wang, W.J.; Jiang, W.J.; Wang, H.Y.; Liu, Q.Y.; Zhu, M.H.; Jin, X.S. Experimental Study on the Wear and Damage Behavior of Different Wheel/Rail Materials. *Proc. Inst. Mech. Eng. Part F J. Rail Rapid Transit* **2016**, *230*, 3–14. [\[CrossRef\]](#)
7. Ma, L.; He, C.G.; Zhao, X.J.; Guo, J.; Zhu, Y.; Wang, W.J.; Liu, Q.Y.; Jin, X.S. Study on Wear and Rolling Contact Fatigue Behaviors of Wheel/Rail Materials under Different Slip Ratio Conditions. *Wear* **2016**, *366–367*, 13–26. [\[CrossRef\]](#)
8. Rocha, R.C.; Ewald, H.; Rezende, A.B.; Fonseca, S.T.; Mei, P.R. Using twin disc for applications in the railway: A systematic review. *J. Braz. Soc. Mech. Sci. Eng.* **2023**, *45*, 191. [\[CrossRef\]](#)
9. Jendel, T.; Berg, M. Prediction of Wheel Profile Wear: Methodology and Verification. *Veh. Syst. Dyn.* **2003**, *37*, 502–513. [\[CrossRef\]](#)
10. Faccoli, M.; Zani, N.; Ghidini, A.; Petrogalli, C. Experimental and numerical investigation on the wear behavior of high performance railway wheel steels paired with various brake block materials under dry sliding conditions. *Wear* **2022**, *506–507*, 204456. [\[CrossRef\]](#)
11. Provezza, L.; Bodini, I.; Petrogalli, C.; Lancini, M.; Solazzi, L.; Faccoli, M. Monitoring the Damage Evolution in Rolling Contact Fatigue Tests Using Machine Learning and Vibrations. *Metals* **2021**, *11*, 283. [\[CrossRef\]](#)
12. Bruni, S.; Collina, A.; Diana, G.; Vanolo, P. Lateral dynamics of a railway vehicle in tangent track and curve: Tests and simulation. *Veh. Syst. Dyn.* **2000**, *33*, 464–477. [\[CrossRef\]](#)
13. Braghin, F.; Bruni, S.; Resta, F. Wear of railway wheel profiles: A comparison between experimental results and a mathematical model. *Veh. Syst. Dyn.* **2003**, *37*, 478–489. [\[CrossRef\]](#)
14. Iwnicki, S. Simulation of wheel—Rail contact forces. *Fatigue Fract. Eng. Mater. Struct.* **2003**, *26*, 887–900. [\[CrossRef\]](#)
15. Ye, Y.; Huang, C.; Zeng, J.; Wang, S.; Liu, C.; Li, F. Predicting Railway Wheel Wear by Calibrating Existing Wear Models: Principle and Application. *Reliab. Eng. Syst. Saf.* **2023**, *238*, 109462. [\[CrossRef\]](#)
16. Kang, X.; Chen, G.; Chen, X.; Deng, C.; Ma, Y.; Zhao, Y.; Lu, S. Analysis of the Generation Mechanism and Evolution of the Wheel High-Order Polygonal Wear of Subway Trains. *Eng. Fail. Anal.* **2023**, *151*, 107375. [\[CrossRef\]](#)
17. Ao, N.; Zhang, X.; Zhao, X.; Hu, F.; Jian, B.; Wu, S. Remaining Fatigue Life Assessment of High-Speed Railway Wheel Web under Measured Load Spectra. *Eng. Fract. Mech.* **2024**, *295*, 109813. [\[CrossRef\]](#)
18. Sang, H.; Zeng, J.; Qi, Y.; Mu, J.; Gan, F. Study on Wheel Wear Mechanism of High-Speed Train in Accelerating Conditions. *Wear* **2023**, *516–517*, 204597. [\[CrossRef\]](#)
19. de Paula Pacheco, P.A.; Endlich, C.S.; Vieira, K.L.S.; Reis, T.; dos Santos, G.F.M.; dos Santos Júnior, A.A. Optimization of Heavy Haul Railway Wheel Profile Based on Rolling Contact Fatigue and Wear Performance. *Wear* **2023**, *522*, 204704. [\[CrossRef\]](#)

20. Kato, T.; Kato, H.; Makino, T. Effect of Elevated Temperature on Shelling Property of Railway Wheel Steel. *Wear* **2016**, *366*–367, 359–367. [\[CrossRef\]](#)
21. Makino, T.; Kato, T.; Hirakawa, K. Review of the fatigue damage tolerance of high-speed railway axles in Japan. *Eng. Fract. Mech.* **2011**, *78*, 810–825. [\[CrossRef\]](#)
22. Mazzù, A.; Petrogalli, C.; Lancini, M.; Ghidini, A.; Faccoli, M. Effect of Wear on Surface Crack Propagation in Rail–Wheel Wet Contact. *J. Mater. Eng. Perform.* **2018**, *27*, 630–639. [\[CrossRef\]](#)
23. Faccoli, M.; Petrogalli, C.; Lancini, M.; Ghidini, A.; Mazzù, A. Rolling Contact Fatigue and Wear Behavior of High-Performance Railway Wheel Steels Under Various Rolling-Sliding Contact Conditions. *J. Mater. Eng. Perform.* **2017**, *26*, 3271–3284. [\[CrossRef\]](#)
24. Gutsulyak, D.V.; Stanlake, L.J.E.; Qi, H. Twin Disc Evaluation of Third Body Materials in the Wheel/Rail Interface. *Tribol.-Mater. Surf. Interfaces* **2021**, *15*, 115–126. [\[CrossRef\]](#)
25. Wang, W.J.; Zhang, H.F.; Wang, H.Y.; Liu, Q.Y.; Zhu, M.H. Study on the Adhesion Behavior of Wheel/Rail under Oil, Water and Sanding Conditions. *Wear* **2011**, *271*, 2693–2698. [\[CrossRef\]](#)
26. Faccoli, M.; Petrogalli, C.; Lancini, M.; Ghidini, A.; Mazzù, A. Effect of desert sand on wear and rolling contact fatigue behaviour of various railway wheel steels. *Wear* **2018**, *396*–397, 146–161. [\[CrossRef\]](#)
27. Grieve, D.G.; Dwyer-Joyce, R.S.; Beynon, J.H. Abrasive wear of railway track by solid contaminants. *Proc. Inst. Mech. Eng. Part F J. Rail Rapid Transit* **2001**, *215*, 193–205. [\[CrossRef\]](#)
28. Omasta, M.; Machatka, M.; Smejkal, D.; Hartl, M.; Křupka, I. Influence of sanding parameters on adhesion recovery in contaminated wheel–rail contact. *Wear* **2015**, *322*–323, 218–225. [\[CrossRef\]](#)
29. Lewis, R.; Dwyer-Joyce, R.S. Wear at the wheel/rail interface when sanding is used to increase adhesion. *Proc. Inst. Mech. Eng. Part F J. Rail Rapid Transit* **2006**, *220*, 29–41. [\[CrossRef\]](#)
30. Skipper, W.A.; Chalisey, A.; Lewis, R. Particle characterisation of rail sand for understanding tribological behaviour. In Proceedings of the 11th International Conference on Contact Mechanics and Wear of Rail/Wheel Systems, Delft, The Netherlands, 27–28 September 2018; pp. 886–895.
31. Mazzù, A.; Ghidini, A.; Zani, N.; Faccoli, M. A simplified numerical study of wheel/rail material coupling in presence of solid contaminants. *Tribol.—Mater. Surf. Interfaces* **2021**, *15*, 102–114. [\[CrossRef\]](#)
32. Mazzù, A.; Ghidini, A.; Zani, N.; Faccoli, M. Study of wheel/rail material coupling in presence of solid contaminants. In Proceedings of the 11th International Conference on Contact Mechanics and Wear of Rail/Wheel Systems, Delft, The Netherlands, 27–28 September 2018; pp. 701–710.
33. Suhr, B.; Skipper, W.A.; Lewis, R.; Six, K. Sanded Wheel–Rail Contacts: Experiments on Sand Crushing Behaviour. *Lubricants* **2023**, *11*, 38. [\[CrossRef\]](#)
34. Shi, Z.; Nencioni, L.; Meli, E.; Ding, H.; Wang, W.; Andrea, R. Effect of Material Hardness Ratio on Wear and Rolling Contact Fatigue: Development and Validation of New Laws. *Wear* **2023**, *514*–515, 204561. [\[CrossRef\]](#)
35. He, C.G.; Huang, Y.B.; Ma, L.; Guo, J.; Wang, W.J.; Liu, Q.Y.; Zhu, M.H. Experimental Investigation on the Effect of Tangential Force on Wear and Rolling Contact Fatigue Behaviors of Wheel Material. *Tribol. Int.* **2015**, *92*, 307–316. [\[CrossRef\]](#)
36. Guo, L.C.; Zhu, W.T.; Shi, L.B.; Liu, Q.Y.; Cai, Z.B.; Wang, W.J. Study on Wear Transition Mechanism and Wear Map of CL60 Wheel Material under Dry and Wet Conditions. *Wear* **2019**, *426*–427, 1771–1780. [\[CrossRef\]](#)
37. Qiu, C.; Cookson, J.; Mutton, P. The role of microstructure and its stability in performance of wheels in heavy haul service. *J. Mod. Transp.* **2017**, *25*, 261–267. [\[CrossRef\]](#)
38. Stock, R.; Oldknow, K.; Magel, E. Addressing Perceptions Regarding the Influence of Relative Hardness on Wheel/Rail Performance. *Wear* **2024**, *538*–539, 205225. [\[CrossRef\]](#)
39. Viáfara, C.C.; Castro, M.I.; Vélez, J.M.; Toro, A. Unlubricated sliding wear of pearlitic and bainitic steels. *Wear* **2005**, *259*, 405–411. [\[CrossRef\]](#)
40. Zani, N.; Chaise, T.; Ghidini, A.; Faccoli, M.; Mazzù, A. Numerical study about the effect of bainitic traces on plasticity in ferritic-pearlitic railway wheels. *Proc. Inst. Mech. Eng. Part. F J. Rail Rapid Transit* **2020**, *235*, 726–740. [\[CrossRef\]](#)
41. Faccoli, M.; Zani, N.; Ghidini, A.; Petrogalli, C. Tribological Behavior of Two High Performance Railway Wheel Steels Paired with a Brake Block Cast Iron. *Tribol. Trans.* **2021**, *65*, 296–307. [\[CrossRef\]](#)
42. Miranda, R.S.; Rezende, A.B.; Fonseca, S.T.; Fernandes, F.M.; Sinatora, A.; Mei, P.R. Fatigue and Wear Behavior of Pearlitic and Bainitic Microstructures with the Same Chemical Composition and Hardness Using Twin-Disc Tests. *Wear* **2022**, *494*–495, 204253. [\[CrossRef\]](#)
43. Ishikawa, N.; Yasuda, K.; Sueyoshi, H.; Endo, S.; Ikeda, H.; Morikawa, T.; Higashida, K. Microscopic Deformation and Strain Hardening Analysis of Ferrite-Bainite Dual-Phase Steels Using Micro-Grid Method. *Acta Mater.* **2015**, *97*, 257–268. [\[CrossRef\]](#)
44. Seo, J.W.; Hur, H.M.; Kwon, S.J. Effect of Mechanical Properties of Rail and Wheel on Wear and Rolling Contact Fatigue. *Metals* **2022**, *12*, 630. [\[CrossRef\]](#)
45. Seo, J.-W.; Kwon, S.-J.; Jun, H.-K.; Lee, C.-W. Effects of Wheel Materials on Wear and Fatigue Damage Behaviors of Wheels/Rails. *Tribol. Trans.* **2019**, *62*, 635–649. [\[CrossRef\]](#)
46. Zeng, D.; Qiao, S.; Chen, X.; Gong, Y.; Jiang, B.; Zhao, H.; Zhang, J.; Lu, L. Rolling Contact Fatigue and Wear Behavior of a Vanadium Microalloyed Railway Wheel Steel under Dry Rolling / Sliding Condition. *Int. J. Fatigue* **2024**, *182*, 108207. [\[CrossRef\]](#)
47. Cao, X.; Huang, W.L.; He, C.G.; Peng, J.F.; Guo, J.; Wang, W.J.; Liu, Q.Y.; Zhu, M.H. The effect of alumina particle on improving adhesion and wear damage of wheel/rail under wet conditions. *Wear* **2016**, *348*–349, 98–115. [\[CrossRef\]](#)

48. Viesca, J.L.; González-Cachón, S.; García, A.; González, R.; Bernardo-Sánchez, A.; Hernández Battez, A. Influence of Environmental Conditions and Oxidation on the Coefficient of Friction Using Microalloyed Rail Steels. *Proc. Inst. Mech. Eng. Part F J. Rail Rapid Transit* **2020**, *235*, 353–360. [\[CrossRef\]](#)
49. Chen, H. Review of Various Influencing Factors and Improvement Measures on Wheel-Rail Adhesion. *Wear* **2024**, *in press*. [\[CrossRef\]](#)
50. Shi, L.B.; Ma, L.; Guo, J.; Liu, Q.Y.; Zhou, Z.R.; Wang, W.J. Influence of Low Temperature Environment on the Adhesion Characteristics of Wheel-Rail Contact. *Tribol. Int.* **2018**, *127*, 59–68. [\[CrossRef\]](#)
51. Liu, C.-P.; Liu, P.-T.; Pan, J.-Z.; Chen, C.-H.; Ren, R.-M. Effect of Original Microstructure on Wear Property of ER9 Wheel Steel. *Ironmak. Steelmak.* **2021**, *48*, 133–141. [\[CrossRef\]](#)
52. Shen, M.X.; Qin, Y.F.; Ji, D.H.; Yu, M.; Li, S.X.; Huangfu, L.; Liu, S.P. Role of Ambient Temperature in the Adhesion and Damage Characteristics of Wheel/Rail Interface during Rolling-Sliding Contact. *Wear* **2022**, *506–507*, 204458. [\[CrossRef\]](#)
53. Nakahara, T.; Baek, K.S.; Chen, H.; Ishida, M. Relationship between Surface Oxide Layer and Transient Traction Characteristics for Two Steel Rollers under Unlubricated and Water Lubricated Conditions. *Wear* **2011**, *271*, 25–31. [\[CrossRef\]](#)
54. Rahaman, M.L.; Bernal, E.; Spiryagin, M.; Bosomworth, C.; Sneath, B.; Wu, Q.; Cole, C.; McSweeney, T. An Investigation into the Effect of Slip Rate on the Traction Coefficient Behaviour with a Laboratory Replication of a Locomotive Wheel Rolling/Sliding along a Railway Track. *Tribol. Int.* **2023**, *187*, 108773. [\[CrossRef\]](#)
55. Chen, M.; Zhai, W.; Sun, Y. Investigation on effect of wheel polygonal wear on high-speed vehicle-track-subgrade interaction based on green function method. In Proceedings of the 11th International Conference on Contact Mechanics and Wear of Rail/Wheel Systems, Delft, The Netherlands, 27–28 September 2018; pp. 147–154.
56. Shi, M.; Li, W.; Wu, M.; Shen, G. Analysis of Out-of-Round Wheels and the Effect of Wheel Polygonalization on Vehicle Vibration. In Proceedings of the 11th International Conference on Contact Mechanics and Wear of Rail/Wheel Systems, Delft, The Netherlands, 27–28 September 2018; pp. 856–861.
57. Fu, B.; Bruni, S.; Luo, S. Numerical simulation for polygonal wear of railway wheels. In Proceedings of the 11th International Conference on Contact Mechanics and Wear of Rail/Wheel Systems, Delft, The Netherlands, 27–28 September 2018; pp. 271–280.
58. Niu, Z.; Pang, F.; Zhang, X.; Du, T.; Su, J. Study on the Influence of Wheel Polygon on the Vibration Characteristics of Bogie System. *Vib. Proced.* **2022**, *44*, 47–53. [\[CrossRef\]](#)
59. Ye, Y.; Zhu, B.; Huang, P.; Peng, B. OORNet: A Deep Learning Model for on-Board Condition Monitoring and Fault Diagnosis of out-of-Round Wheels of High-Speed Trains. *Meas. J. Int. Meas. Confed.* **2022**, *199*, 111268. [\[CrossRef\]](#)
60. Ding, H.; Mu, X.; Zhu, Y.; Yang, W.; Xiao, Q.; Wang, W.; Liu, Q.; Guo, J.; Zhou, Z. Effect of Laser Claddings of Fe-Based Alloy Powder with Different Concentrations of WS2 on the Mechanical and Tribological Properties of Railway Wheel. *Wear* **2022**, *488–489*, 204174. [\[CrossRef\]](#)
61. Lewis, S.R.; Lewis, R.; Fletcher, D.I. Assessment of Laser Cladding as an Option for Repairing/Enhancing Rails. *Wear* **2015**, *330–331*, 581–591. [\[CrossRef\]](#)
62. Wang, X.; Lei, L.; Yu, H. A Review on Microstructural Features and Mechanical Properties of Wheels/Rails Cladded by Laser Cladding. *Micromachines* **2021**, *12*, 152. [\[CrossRef\]](#)
63. Lu, P.; Lewis, S.R.; Fretwell-Smith, S.; Engelberg, D.L.; Fletcher, D.I.; Lewis, R. Laser Cladding of Rail; the Effects of Depositing Material on Lower Rail Grades. *Wear* **2019**, *438–439*, 203045. [\[CrossRef\]](#)
64. Roy, T.; Lai, Q.; Abrahams, R.; Mutton, P.; Paradowska, A.; Soodi, M.; Yan, W. Effect of Deposition Material and Heat Treatment on Wear and Rolling Contact Fatigue of Laser Cladded Rails. *Wear* **2018**, *412–413*, 69–81. [\[CrossRef\]](#)
65. Ekberg, A.; Åkesson, B.; Kabo, E. Wheel/rail rolling contact fatigue—Probe, predict, prevent. *Wear* **2014**, *314*, 2–12. [\[CrossRef\]](#)
66. Ghidini, A.; Diener, M.; Mazzù, A.; Zani, N.; Petrogalli, C.; Faccoli, M. Considerations about Microstructure of Solid Wheels with Traces of Bainite Considerazioni Sulla Microstruttura Di Ruote Monoblocco Con Tracce Di Bainite. *Ing. Ferrovi.* **2019**, *75*, 162–178.
67. Akama, M.; Kimata, T. Numerical Simulation Model for the Competition between Short Crack Propagation and Wear in the Wheel Tread. *Wear* **2020**, *448–449*, 203205. [\[CrossRef\]](#)
68. Wang, H.H.; Wang, W.J.; Han, Z.Y.; Wang, Y.; Ding, H.H.; Lewis, R.; Lin, Q.; Liu, Q.Y.; Zhou, Z.R. Wear and Rolling Contact Fatigue Competition Mechanism of Different Types of Rail Steels under Various Slip Ratios. *Wear* **2023**, *522*, 204721. [\[CrossRef\]](#)
69. Magel, E.; Mutton, P.; Ekberg, A.; Kapoor, A. Rolling Contact Fatigue, Wear and Broken Rail Derailments. *Wear* **2016**, *366–367*, 249–257. [\[CrossRef\]](#)
70. Bolton, P.J.; Clayton, P. Rolling-sliding wear damage in rail and tyre steels. *Wear* **1984**, *93*, 145–165. [\[CrossRef\]](#)
71. Lewis, R.; Olofsson, U. Mapping rail wear regimes and transitions. *Wear* **2004**, *257*, 721–729. [\[CrossRef\]](#)
72. Beagley, T.M. Severe wear of rolling/sliding contacts. *Wear* **1976**, *36*, 317–335. [\[CrossRef\]](#)
73. Zakharov, S.; Komarovskiy, I.; Zharov, I. Wheel flange/rail head wear simulation. *Wear* **1998**, *215*, 18–24. [\[CrossRef\]](#)
74. Danks, D.; Clayton, P. Comparison of the wear process for eutectoid rail steels: Field and laboratory tests. *Wear* **1987**, *120*, 233–250. [\[CrossRef\]](#)
75. Ding, H.H.; He, C.G.; Ma, L.; Guo, J.; Liu, Q.Y.; Wang, W.J. Wear Mapping and Transitions in Wheel and Rail Materials under Different Contact Pressure and Sliding Velocity Conditions. *Wear* **2016**, *352–353*, 1–8. [\[CrossRef\]](#)
76. Xie, Y.; Wang, W.; Guo, J.; An, B.; Chen, R.; Wu, Q.; Bernal, E.; Ding, H.; Spiryagin, M. Rail Rolling Contact Fatigue Response Diagram Construction and Shakedown Map Optimization. *Wear* **2023**, *528–529*, 204964. [\[CrossRef\]](#)

77. Zhu, W.T.; Guo, L.C.; Shi, L.B.; Cai, Z.B.; Li, Q.L.; Liu, Q.Y.; Wang, W.J. Wear and Damage Transitions of Two Kinds of Wheel Materials in the Rolling-Sliding Contact. *Wear* **2018**, 398–399, 79–89. [\[CrossRef\]](#)
78. Zhou, L.; Wang, W.J.; Hu, Y.; Marconi, S.; Meli, E.; Ding, H.H.; Liu, Q.Y.; Guo, J.; Rindi, A. Study on the Wear and Damage Behaviors of Hypereutectoid Rail Steel in Low Temperature Environment. *Wear* **2020**, 456–457, 203365. [\[CrossRef\]](#)
79. Zapata, D.; Jaramillo, J.; Toro, A. Rolling Contact and Adhesive Wear of Bainitic and Pearlitic Steels in Low Load Regime. *Wear* **2011**, 271, 393–399. [\[CrossRef\]](#)
80. Ashby, M.F.; Lim, S.C. Wear-mechanism maps. *Scr. Metall. Mater.* **1990**, 24, 805–810. [\[CrossRef\]](#)
81. Archard, J.F. Contact and rubbing of flat surfaces. *J. Appl. Phys.* **1953**, 24, 981–988. [\[CrossRef\]](#)
82. Makino, T.; Kato, T.; Hirakawa, K. The effect of slip ratio on the rolling contact fatigue property of railway wheel steel. *Int. J. Fatigue* **2012**, 36, 68–79. [\[CrossRef\]](#)
83. Vakkalagadda, M.R.K.; Vineesh, K.P. Causes and Failure Forms of Railway Wheels. *Mater. Today Proc.* **2023**, in press. [\[CrossRef\]](#)
84. Ancellotti, S.; Benedetti, M.; Dallago, M.; Fontanari, V. Fluid Pressurization and Entrapment Effects on the SIFs of Cracks Produced under Lubricated Rolling-Sliding Contact Fatigue. *Procedia Struct. Integr.* **2016**, 2, 3098–3108. [\[CrossRef\]](#)
85. Zani, N.; Ekh, M.; Ekberg, A.; Mazzù, A. Application of a semianalytical strain assessment and multiaxial fatigue analysis to compare rolling contact fatigue in twin-disk and full-scale wheel/rail contact conditions. *Fatigue Fract. Eng. Mater. Struct.* **2022**, 45, 222–238. [\[CrossRef\]](#)
86. Beretta, S.; Donzella, G.; Roberti, R.; Ghidini, A. Contact fatigue propagation of deep defects in railway wheels. In Proceedings of the 13th European Conference on Fracture-ECF13, CD-ROM, San Sebastian, Spain, 6–9 September 2000; Elsevier: Oxford, UK, 2000; pp. 147–154.
87. Kato, T.; Fujimura, T.; Yamamoto, Y.; Dedmon, S.; Hiramatsu, S.; Kato, H.; Kimura, Y.; Pilch, J. Critical Internal Defect Size for Subsurface Crack Initiation in Heavy Haul Car Wheels. *Wear* **2019**, 438–439, 203038. [\[CrossRef\]](#)
88. Zeng, D.; Lu, L.; Zhang, J.; Jin, X.; Zhu, M. Effect of Micro-Inclusions on Subsurface-Initiated Rolling Contact Fatigue of a Railway Wheel. *Proc. Inst. Mech. Eng. Part F J. Rail Rapid Transit* **2016**, 230, 544–553. [\[CrossRef\]](#)
89. Zeng, D.; Xu, T.; Wang, J.; Lu, L.; Meng, W.; Jiang, B.; Zou, Q. Investigation of the Crack Initiation of Subsurface Rolling Contact Fatigue in Railway Wheels. *Int. J. Fatigue* **2020**, 130, 105281. [\[CrossRef\]](#)
90. Johnson, K.L. *Contact Mechanics*; Cambridge University Press: Cambridge, UK, 1985.
91. Lewis, R.; Olofsson, U. *Wheel-Rail Interface Handbook*; Elsevier: Amsterdam, The Netherlands, 2009.
92. Foletti, S.; Desimone, H.J. Application of Shakedown Maps under Variable Loads. *Eng. Fract. Mech.* **2007**, 74, 527–538. [\[CrossRef\]](#)
93. Zhang, S.; Liu, Q.; Spiriyagin, M.; Wu, Q.; Ding, H.; Wen, Z.; Wang, W. Gaps, Challenges and Possible Solution for Prediction of Wheel–Rail Rolling Contact Fatigue Crack Initiation. *Railw. Eng. Sci.* **2023**, 31, 207–232. [\[CrossRef\]](#)
94. Salas Vicente, F.; Pascual Guillamón, M. Use of the fatigue index to study rolling contact wear. *Wear* **2019**, 436–437, 203036. [\[CrossRef\]](#)
95. Zani, N.; Petrogalli, C. Predictive maps for the rolling contact fatigue and wear interaction in railway wheel steels. *Wear* **2022**, 510–511, 204513. [\[CrossRef\]](#)
96. M-107/208; AAR Manual of Standards and Recommended Practices Wheels and Axles. American Association of Railroads: Washington, DC, USA, 2011.
97. Ghidini, A.; Faccoli, M.; Mazzù, A. *SANDLOS® Wheels for Desert Environments*; Lucchini RS: Lovere, BG, Italy, 2017.
98. EN 13262; Railway Applications—Wheelsets and Bogies—Wheels—Product Requirements. European Committee for Standardization: Brussels, Belgium, 2011.
99. Ghidini, A.; Diener, M.; Gianni, A.; Schneider, J. *SUPERLOS® Innovative Steel by Lucchini RS for High-Speed Wheel Application*; Lucchini RS: Lovere, BG, Italy, 2017.
100. EN 13674-1; Railway Applications—Track—Rail—Part 1: Vignole Railway Rails 46 kg/m and above; Norm. CEN, European Committee for Standardization: Brussels, Belgium, 2011.
101. UNI EN 13925-2; Non-Destructive Testing—X-Ray Diffraction from Polycrystalline and Amorphous Materials—Part 2: Procedures. Ente Nazionale Italiano di Normazione: Milan, Italy, 2006.
102. Santa, J.F.; Cuervo, P.; Christoforou, P.; Harmon, M.; Beagles, A.; Toro, A.; Lewis, R. Twin Disc Assessment of Wear Regime Transitions and Rolling Contact Fatigue in R400HT—E8 Pairs. *Wear* **2019**, 432–433, 102916. [\[CrossRef\]](#)
103. Bodini, I.; Zani, N.; Petrogalli, C.; Mazzù, A.; Kato, T.; Makino, T. Damage Assessment in a Wheel Steel under Alternated Dry-Lubricated Contact by an Innovative Vision System. *Wear* **2023**, 530–531, 205064. [\[CrossRef\]](#)

Disclaimer/Publisher’s Note: The statements, opinions and data contained in all publications are solely those of the individual author(s) and contributor(s) and not of MDPI and/or the editor(s). MDPI and/or the editor(s) disclaim responsibility for any injury to people or property resulting from any ideas, methods, instructions or products referred to in the content.